Preparation, characterization and activity of CuZn and Cu2 superoxide dismutase mimics encapsulated in mesoporous silica

Matías Patriarca, Veronica Daier, Gerardo Camí, Eric Rivière, Christelle Hureau, Sandra Signorella

Preparation, Characterization and Activity of CuZn and Cu_2 Superoxide Dismutase Mimics Encapsulated in Mesoporous Silica

Matías Patriarca,[a] Verónica Daier,[a] Gerardo Camí,[a] Eric Rivière,[b] Christelle Hureau,[c] and Sandra Signorella[a,*]

[a]*IQUIR (Instituto de Química Rosario), Consejo Nacional de Investigaciones Científicas y Técnicas (CONICET), Facultad de Ciencias Bioquímicas y Farmacéuticas, Universidad Nacional de Rosario, Suipacha 531, S2002LRK Rosario, Argentina*

[b]*Institut de Chimie Moléculaire et des Matériaux d'Orsay, CNRS, Université Paris Sud, Université Paris Saclay, 91405 Orsay Cedex, France*

[c]*CNRS, LCC (Laboratoire de Chimie de Coordination) and UPS, INPT, LCC, Université de Toulouse, 205 route de Narbonne, F-31077 Toulouse, France*

*Corresponding author: signorella@iquir-conicet.gov.ar

Abstract

Encapsulation of three superoxide dismutase (SOD) functional mimics, $[CuZn(dien)_2(\mu\text{-}Im)(ClO_4)_2]ClO_4$ (**1**), $[Cu_2(dien)_2(\mu\text{-}Im)(ClO_4)_2]ClO_4$ (**2**) (Im = imidazolate, dien = diethylenetriamine), and $[CuZn(salpn)Cl_2]$ (**3**) (H_2salpn = 1,3-bis(salicylideneamino)propane) in mesoporous MCM-41 silica afforded three hybrid catalysts **1**@MCM-41, **2**@MCM-41 and **3**@MCM-41. Spectroscopic and magnetic analyses of these materials confirmed the metal centers of the complexes keep the coordination sphere after insertion into the MCM-41 silica matrix. For the imidazolate-bridged complexes the silica channels restraint the relative orientation of the two metal ions. While **3**@MCM-41 shows SOD activity significantly lower than the host-free complex, insertion of the imidazolate-bridged CuZn or Cu_2 complexes by ion exchange onto mesoporous MCM-41 silica affords durable and recoverable supported catalysts with much better SOD activity than the free complexes. For confined imidazolate-bridged complexes, **1**@MCM-41 and **2**@MCM-41, the small pore size of the silica matrix improves the SOD activity more than a host with larger pores. This high SOD activity is attributed to the close-fitting of the complexes into the nanochannels of MCM-41 silica that favors the Cu active site and HImZn(or Cu) group stay in close proximity during catalysis.

Keywords

Biomimics; encapsulated CuZn complexes; mesoporous MCM-41 silica; SOD activity

1. INTRODUCTION

Superoxide dismutase (SOD) enzymes are part of the first line of defense of most organisms to remove superoxide radical anion ($O_2^{\bullet-}$) formed as a byproduct during the normal cell respiration [1]. This radical anion is the primary source of undesired harmful species like H_2O_2 and $HO^{\bullet}$ [2], and in certain pathologies such as inflammation, neurodegenerative disorders and strokes, its production exceeds the amount of SOD available and damages the body tissues [3,4]. CuZn-SOD, with an imidazolate-bridged CuZn active site, is a very efficient catalyst for $O_2^{\bullet-}$ removal found in the cytosol, nucleus, peroxisomes, and mitochondrial intermembrane space of eukaryotic cells and in the periplasmic space of bacteria [5]. However, administration of exogenous SOD has not been successful for therapeutic treatment mainly because of the extremely short half-life of the enzyme and its high molecular weight that prevent it to enter the cells [6,7]. To circumvent the unfavorable bioavailability of the enzyme, pharmacological research has pointed at the development of low molecular weight SOD mimics that can overcome the enzyme immunogenicity and tissue permeability [8,9]. However, in aqueous solution these artificial catalysts can suffer hydrolysis, metal dissociation or oligomerization. The insertion of the catalyst inside a porous matrix can confer confinement and isolation of the metal center avoiding undesired interactions and improve the complex stability [10-12]. In a certain way, the solid matrix channels should play the role of the protein framework of the enzyme. Encapsulation of SOD mimics in the mesoporous material shares advantageous features of both heterogeneous (hardiness, easy separation) and homogeneous (well defined structure that can be correlated to activity) catalysts. In particular, mesoporous silicas possess an ordered mesostructure with high specific area and pore volume and, consequently, high adsorption capability, are biocompatible at practical concentrations and can act as effective drug delivery systems [11, 13-14]. The modulation of the pore size and the surface properties convert them in ideal materials for hosting molecules of different dimensions, shapes and functionalities [15-17]. In the case of single-bridged dinuclear complexes, the space confinement can prevent

separation of the metal centers [18]. The reduction of the pore size of the host has proved to be beneficial for SOD activity of biomimetic catalysts [19], although too small pores caused the opposite effect [20-21]. Therefore, the SOD activity of the mimics can be modulated by fine-tuning the pore width of the mesoporous matrix.

We have previously reported the SOD activity of CuZn and Cu_2 mimics and showed that their intrinsic activity was enhanced several times on encapsulation in mesoporous SBA-15 silica [22]. This silica had pore size distribution around 8.6 nm, about 7 times larger than the complexes. Since the complexes are retained inside the channels via ionic interactions and pore restrictions, we decided to examine the effect of encapsulation of these active mimics in mesoporous silica with smaller pore size. In this work we prepared a well ordered mesoporous MCM-41 silica with pore diameter of 3.4 nm that fits the complexes closer than SBA-15, and evaluated the SOD activity of three SOD mimics, $[CuZn(dien)_2(\mu\text{-Im})(ClO_4)_2]ClO_4$ (**1**), $[Cu_2(dien)_2(\mu\text{-Im})(ClO_4)_2]ClO_4$ (**2**) (Im = imidazolate, dien = diethylenetriamine), and $[CuZn(salpn)Cl_2]$ (**3**) (H_2salpn = 1,3-bis(salicylideneamino)propane) [23], shown in Figure 1, encapsulated in the MCM-41 silica, aimed at assessing the role of the pore size on the SOD activity of these hybrid materials.

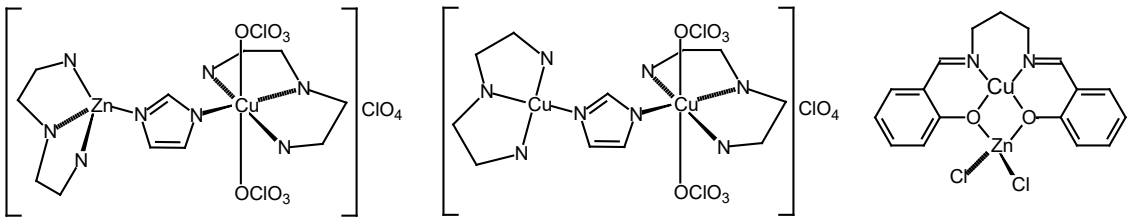

1 **2** **3**

Figure 1. Complexes used in this work

2. EXPERIMENTAL PART

2.1. Materials

All reagents were used as received, without further purification. $[CuZn(dien)_2(\mu\text{-}Im)(ClO_4)_2]ClO_4$ (**1**), $[Cu_2(dien)_2(\mu\text{-}Im)(ClO_4)_2]ClO_4$ (**2**), and $[CuZn(salpn)Cl_2]$ (**3**) were synthesized as previously described in reference 23 and have correct analyses (given in SI). Solvents were purified by standard procedures.

2.2. Synthesis of mesoporous MCM-41 silica

The mesoporous silica was synthetized through a modification of the procedure described by Imai & col. [24-25] employing 98% tetraethyl orthosilicate (TEOS) as Si source, 99% cetyltrimethylammonium bromide (C16TAB) as cationic surfactant and structure directing, and the nonionic triblock copolymer pluronic P-123 to control the particles size. 1.10 g of Pluronic P-123 and 3.09 g of C16TAB were dissolved with stirring in an aqueous solution of HCl (35 mL, pH = 0.5). Then 4.25 ml of TEOS was added dropwise and kept under stirring for 24 h. Afterwards, 0.6 ml of concentrated NH_4OH were added and the solution changed into a white gel. The resulting gel was aged for 24 h, and then dried at 60ºC for one week and finally calcined at 600 °C for 3 h to remove the surfactants.

2.3. Encapsulation of complexes 1 – 3 in mesoporous silica MCM-41

Complexes **1** - **3** were immobilized by ionic exchange. In a typical experiment, 0.3 g of MCM-41 were added to a solution of complex (0.20 mmol) in 20 mL of methanol. The mixture was stirred for 24 h at room temperature, filtered, and washed with methanol. The solid material was re-suspended in methanol and stirred overnight to remove residues. The solid was filtered and dried under vacuum until constant weight. Residual mass (%) at 600ºC: 90.1 (**1**@MCM-41); 87.7 (**2**@MCM-41); 83.2 (**3**@MCM-41). Cu wt

%: 2.0 (**1**@MCM-41); 1.6 (**2**@MCM-41); 3.2 (**3**@MCM-41). Significant IR bands (ν cm^{-1}) for **1**@MCM-41 and **2**@MCM-41: 1080 (Si-O), 795 (Si-O), 463 (Si-O-Si), 1585/1460 (Im), 2953/ 3100 (C-H), 3280 (N-H); **3**@MCM-41: 1080 (Si-O), 795 (Si-O), 463 (Si-O-Si), 1598 (C=N) , 1563/1483 (Ar), 1293 (C-O).

2.4. Physical measurements

UV-visible spectra were registered with a JASCO V-550 spectrophotometer. Electron Paramagnetic Resonance (EPR) spectra of solid samples were obtained on an Elexsys E 500 Bruker spectrometer with a microwave of ~ 9.5 GHz, at 120 K. IR spectra were recorded on a Perkin-Elmer Spectrum One FT-IR spectrophotometer. Metal content was determined with a Perkin Elmer NexION 350X Inductively Coupled plasma (ICP) Mass Spectrometer. Magnetic susceptibility data were collected with a Quantum Design MPMS SQUID susceptometer. Thermogravimetric analyses (TGA) were carried out on a TGA 51 Shimadzu thermogravimetric analyzer and on a Perkin-Elmer Diamond TG/DTA Instrument. Cu and Zn K-edge XANES (X-ray absorption near edge structure) spectra were recorded at the BM30B (FAME) beam line of the European Synchrotron Radiation Facility (ESRF, Grenoble, France) [26]. Porosity and surface area were determined from N_2 adsorption-desorption isotherms obtained at 77 K on a Micrometric ASAP 2020 V4.02 (V4.02 G) apparatus. Further experimental details and data analyses of IR, XANES and sorption isotherms are described in SI.

2.5. Indirect SOD assay

The SOD activity of the free and immobilized complexes was evaluated by measuring the inhibition of the photoreduction of nitro blue tetrazolium (NBT), by a method slightly modified from the originally described by Beauchamps and Fridovich [27]. Reaction of methionine and riboflavin, in the presence of light, is the source of superoxide. The suspensions were prepared in 50 mM phosphate buffer of pH 7.8, riboflavin (3.4 μM), methionine (10 mM), NBT (46 μM) and different amounts of immobilized complexes (0-

100 μM). Riboflavin was last added and the reaction was initiated by illumination of the mixtures with a fluorescent lamp at 25ºC [28]. The reduction of NBT was measured at 560 nm after an illumination period of 15 min. The IC_{50} values were determined from concentration-dependent plots. Control reactions confirm that the compounds did not react directly with NBT or riboflavin. Inhibition percentage was calculated according to: $\{(\Delta Abs/t)_{without\ catalyst} - (\Delta Abs/t)_{with\ catalyst}\} \times 100 / (\Delta Abs/t)_{without\ catalyst}$.

3. RESULTS AND DISCUSSIONS

3.1. Preparation and textural properties of the hybrid materials

Mesoporous MCM-41 silica was prepared by hydrolysis of TEOS in acid medium and subsequent assembly with the surfactant under basic conditions. It is known that the acid promotes hydrolysis of TEOS and decreases the number of residual ethoxy groups that can affect the ordered assembly, while the subsequent addition of ammonia aqueous solution favors the building of well-ordered mesostructures through steady self-assembly of negatively charged silicates and positively charged $C16TAB^+$ micelles. The ordered mesopores arrangement of the synthesized MCM-41 silica was confirmed by the narrow size distribution obtained from N_2-sorption studies (see below). Three hybrid materials **1**@MCM-41, **2**@MCM-41 and **3**@MCM-41 were obtained upon insertion of complexes **1** – **3** into the mesoporous MCM-41 silica through the exchange of silanol protons by complex cations (eq. 1).

$$n\text{-SiOH} + \text{catalyst}^{n+} = (-\text{SiO})_n\text{catalyst} + nH^+ \qquad (1)$$

Figure 2 shows the N_2 adsorption-desorption isotherm at 77 K for MCM-41 silica along with the isotherms of the hybrid materials under study, and Figure S1 displays the pore size distributions. All the samples exhibit type IV isotherms with a steep step above the

relative pressure p/p0 = 0.3 due to capillary condensation in the cylindrical mesopores of MCM-41 [29] and little hysteresis loop as previously observed for other MCM-41 based materials [30]. Encapsulation of the complexes in MCM-41 leaves the overall shape of the Brunauer-Emmett-Teller (BET) curves almost unchanged indicating that the mesoporous structure remains practically unaltered. None of the samples contains any significant amount of micropores and the plateau after the hysteresis loop indicate the absence of meaningful secondary mesoporosity. The major difference is the lowering of the overall nitrogen adsorption volume for the hybrid materials as the surface coverage increases. Therefore, **2**@MCM-41 (Figure 2), with low proportion of complex in the hybrid material (see Table 1, last column), shows overall adsorption volume larger than **1**@MCM-41 and **3**@MCM-41.

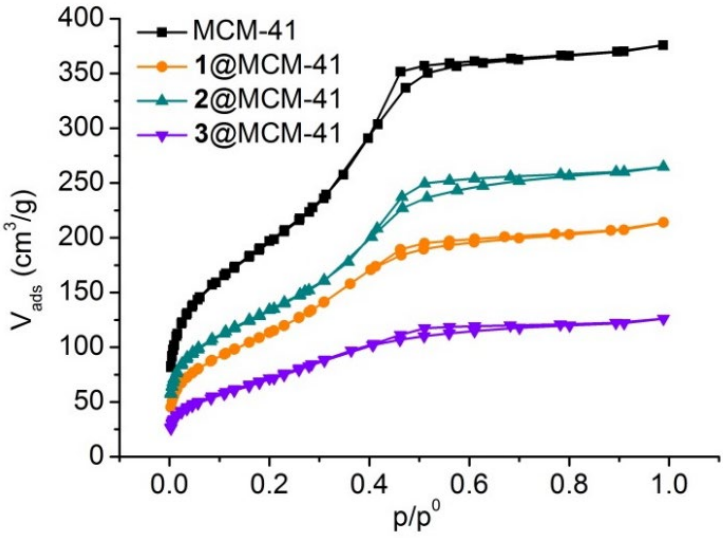

Figure 2. N_2 Adsorption-Desorption Isotherms of mesoporous materials at 77 K

The textural data of all the mesoporous materials are summarized in Table 1. The pore size of pure MCM-41 silica, although small, is suitable for incorporation of complexes **1-3** which are around 1.25 - 1.27 nm wide (calculated from crystal structures [23,31]).

Table 1. Textural properties and amount of complex in the hybrid materials

	S_{BET} [$m^2\ g^{-1}$]	V_{MP} [$cm^3\ g^{-1}$]	V_{TP}[a] [$cm^3\ g^{-1}$]	Wp [nm]	mmol of complex/100 g of material
MCM-41	720	0.51	0.58	3.4	-
1@MCM-41	420	0.27	0.33	2.8	32
2@MCM-41	490	0.34	0.41	3.2	13
3@MCM-41	270	0.15	0.20	2.3	50

[a] $V_{TP} = V_{primary\ MP} + V_{secondary\ MP}$; $V_{\mu P} = 0$; MP = mesopore, μP = micropore

The BET surface area, pore volume and average pore diameter of the hybrid materials decrease compared to pure MCM-41 silica, in agreement with the proportion of complexes inside the channels of MCM-41. The pore size distribution obtained from nitrogen adsorption-desorption isotherms (Figure S1) indicates that the width of the mesopores of MCM-41 have a narrow distribution around 3.4 nm due to the well-ordered arrangement which is retained in the hybrid materials around a lower value.

3.2. Characterization of immobilized complexes

Thermogravimetric analyses of the hybrid materials carried out under oxidative atmosphere (Figure S2) show a first weight loss below 200°C due to the removal of solvent molecules from the silica channels, followed by a second weight loss corresponding to the decomposition of the organic ligands around 275°C for **1**@MCM-41 (8.7%) and **2**@MCM-41 (3.5%) and 425°C for **3**@MCM-41 (14%). The last column of Table 1 lists the amount of complex presents in the hybrid materials, calculated from weight loss data and the results of metal analyses. The lower proportion of **2** encapsulated into the mesoporous silica agrees with the smaller decrease in the pore volume (V_{TP}) and surface area (S_{BET}) measured for this complex.

The FT-IR spectra of the hybrid materials (Figure S3) show strong bands belonging to the Si-O-Si framework and a number of less intense bands characteristic of functional groups present in the ligands (see section 2.3).

Free and immobilized complexes were analyzed by X-ray Absorption Near-Edge Structure (XANES) to check the oxidation state and coordination geometry of the metal centers.

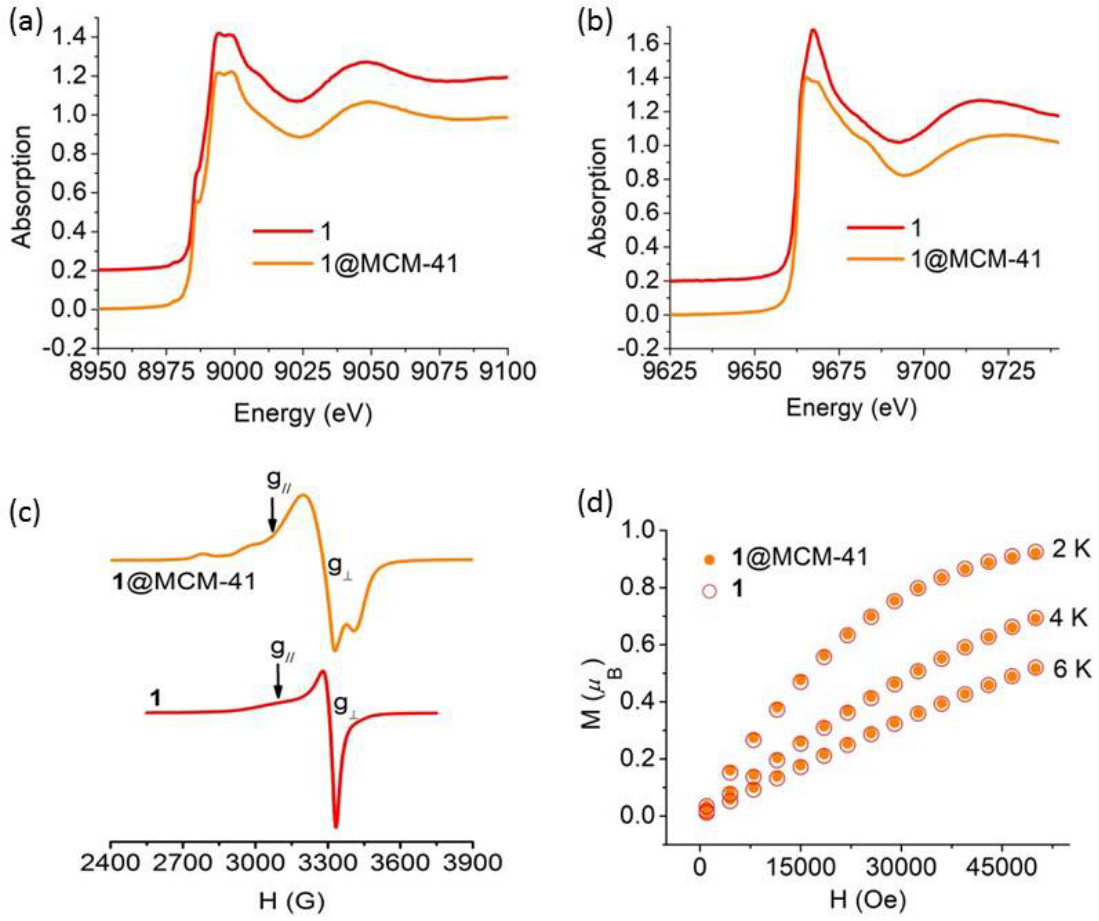

Figure 3. (a) Cu K-edge and (b) Zn K-edge XANES spectra, (c) EPR spectra at *T* = 120 K, and (d) low-temperature magnetic isotherms, of free and encapsulated complex **1**

The Cu K-edge XANES spectra of the three complexes and hybrid materials display characteristic features of square-planar coordinated Cu(II) ion [32-34] and signatures of each complex (as a neat powder or inserted in the material) are virtually superimposable

(Figures 3(a), 4(a) and 5(a)). Therefore, the first-shell environment of the Cu(II) centers is maintained after encapsulation into MCM-41 silica.

The Zn K-edge XANES spectra (Figures 3(b) and 5(b)) of free and immobilized **1** and **3** share a steeply rising edge structure with a maximal normalized absorption intensity of about 1.4 typical of Zn(II) in a distorted tetrahedral geometry [35]. The small difference between the spectra of **1** and **1**@MCM-41 could be due to a slight amount of free Zn(II) ion in the sample of the neat complex [36]. Spectra of **3** and **3**@MCM-41 are almost superimposable confirming encapsulation does not alter the structure of the Zn(II) site, as already observed for **3** inserted in SBA-15 [22].

X-band EPR spectroscopy provided further details on the geometry of the Cu(II) sites in the hybrid materials. **1**@MCM-41 affords a low temperature EPR signal typical of Cu(II) centers with axial symmetry (Figure 3(c), top), with $g_{\perp}$ = 2.06 and $g_{//}$ = 2.21. These *g*-factors are close to those of solid **1** (Figure 3(c), bottom, and Table S1), suggesting the coordination geometry of Cu(II) is retained in the hybrid. Hyperfine splitting in the parallel region of the spectrum of **1**@MCM-41 resolves as a result of the dilution of the complex in the silica matrix, giving $A_{//}$ = 192×10^{-4} cm^{-1}. With these spectral parameters, the *f*-factor ($g_{//}/A_{//}$ ratio), which is useful to examine the tetrahedral distortion of a square planar complex, could be calculated. For square planar complexes *f* varies from 105 to 135 cm, while for tetrahedral complexes $f \sim 250$ [37]. Therefore, higher *f* values imply greater tetrahedral distortion of a tetragonal complex. For **1**@MCM-41, *f* = 115 cm, a characteristic value of Cu(II) in slightly distorted N_4-square planar geometry with a d_{x2-y2} ground state, as also observed for the frozen solution of **1** in dimethyl sulfoxide (*f* = 114 cm) [23].

In the case of **2**, the EPR signal of the powdered neat complex (Figure 4(b), bottom) is broad due to dipolar and spin-spin intermolecular interactions and does not give structural information. In **2**@MCM-41, the paramagnetic centers are diluted in the diamagnetic silica matrix giving a well-defined axial signal with spectral parameters characteristic of tetragonal Cu(II) ions with a d_{x2-y2} ground state: $g_{\perp}$ = 2.03, $g_{//}$ = 2.23, $A_{//}$

= 190×10^{-4} cm^{-1} and f = 117 (Figure 4(b), middle). The lack of ΔM_S = ±1 transitions within the triplet state expected for a coupled Cu(II)$_2$ system indicates that the two copper ions are not interacting, which probably arises from the constrained geometry of the imidazolate-bridged diCu(II) moiety in the channels of the mesoporous silica. The EPR spectrum of **2-dil**@MCM-41, a sample with lower complex loading (8 mmol / 100 g), retains the paramagnetic parameters and affords a better resolved signal (Figure 4(b), top). The value of f = 160 calculated from the EPR parameters of native CuZn-SOD given in Table S1, indicates that the Cu(II) site of the enzyme has tetrahedral distortion higher than the encapsulated complexes.

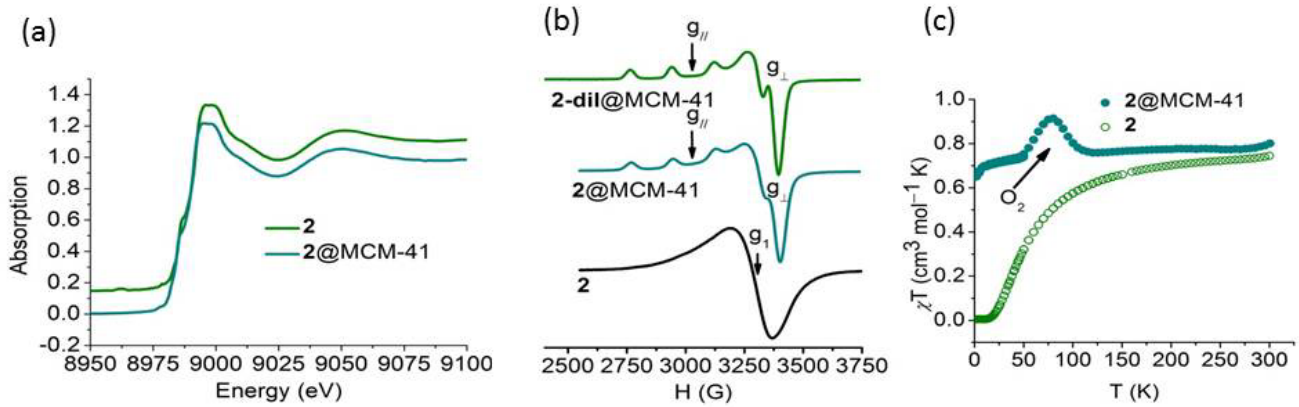

Figure 4. (a) Cu K-edge XANES spectra, (b) EPR spectra at T = 120 K, and (c) $\chi_M T$ vs T plots, of free and encapsulated complex **2**

A solid sample of **3** shows a broad EPR spectrum with the main signal flanked by the ΔM_S = ±1 transitions from the triplet state of a spin-coupled dicopper center that probably results from an aggregation process through π stacking interactions favored by the presence of two aromatic rings in the ligand structure (Figure 5(c), bottom). Insertion of **3** into the channels of the MCM-41 silica yields isolated paramagnetic Cu(II) centers with EPR spectral parameters $g_\perp$ = 2.06, $g_{//}$ = 2.18 characteristic of Cu(II) in a tetragonal environment (Figure 5(c), top). However, the EPR signal of **3**@MCM-41 is still broader

than that of frozen dimethyl sulfoxide solution of **3** suggesting complexes of slightly different geometry could be located in the mesopores.

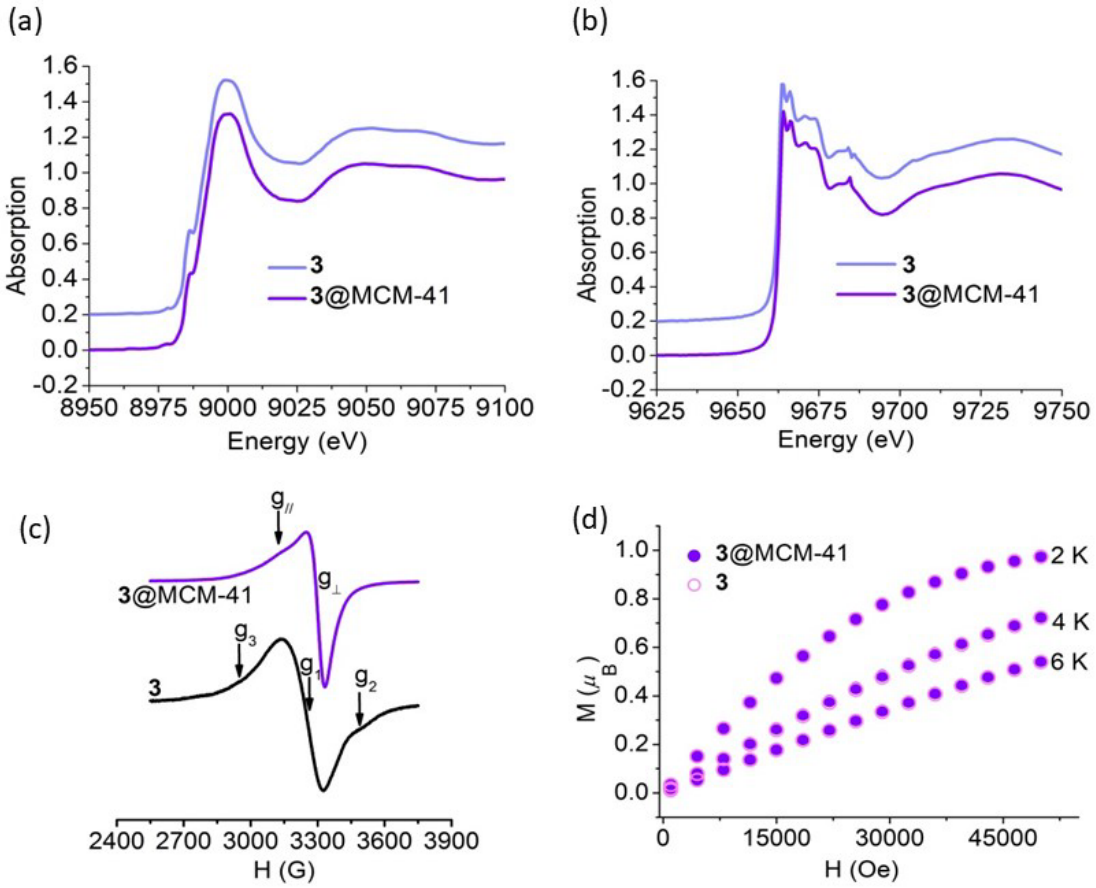

Figure 5. (a) Cu K-edge and (b) Zn K-edge XANES spectra, (c) EPR spectra at T = 120 K, and (d) low-temperature magnetic isotherms, of free and encapsulated complex **3**

Magnetic susceptibility (χ_M) measurements were performed on hybrid materials in the 2 - 300 K temperature range. For **1**@MCM-41 and **3**@MCM-41, the observed $\chi_M T$ values at 300 K were 0.39 and 0.40 $cm^3\ mol^{-1}$ K, respectively, in good agreement with one unpaired electron (S = 1/2), and remained constant over the full range of temperature. Additionally, a good overlap of the low temperature magnetic isotherms of the hybrid materials and neat complexes was observed (Figures 3(d) and 5(d)) confirming the

retention of the complex structure after encapsulation. For **2**@MCM-41, $\chi_M T$ at room temperature (0.78 cm^3 mol^{-1} K) is close to the expected value for two noninteracting Cu(II) centers. As shown in Figure 4(c), $\chi_M T$ remains approximately constant down to ca. 15 K and then decreases to reach a value of 0.66 at 2 K. These results suggest the silica channels restraint the relative orientation of the two Cu(II) ions in such a way that antiferromagnetic interactions are much weaker than in the neat complex (J = - 68.9 cm^{-1} [23]), in accordance with EPR results.

3.3. SOD like activity

Before performing the SOD activity measurements, the stability of the immobilized complexes was checked. To do this, the hybrids materials were incubated in phosphate buffer of pH 7.8 (the medium employed in the SOD tests) for different times, and UV–visible spectra were registered on the supernatant after centrifugation of the suspensions. Spectra taken at different incubation times are shown in Figure S4 together with the spectra of solutions of the free complexes of the same concentration. In all cases, the absorbance increase due to the complex released into the solvent was less than 2% and can correspond to a small fraction of the complexes present near the surface of the material. The hybrid materials used in the SOD tests were pre-treated with phosphate buffer during 15 min, centrifugated and resuspended in the reaction solution to ensure the SOD measurements reflect the activity of the encapsulated complexes without contribution from the complex in solution. The immobilized complexes could be reused several times without significantly losing activity, proving they are the real catalysts and leaching does not occur during the reaction.

The SOD activity of the hybrid materials was evaluated using an indirect assay, which involves inhibition of the reduction of nitro blue tetrazolium (NBT) by $O_2^{\bullet -}$ [38]. In this assay, photoreduced riboflavin reacts with O_2 to generate $O_2^{\bullet -}$ that converts the colorless NBT into purple formazan, measured at 560 nm. The SOD activity of the catalysts is

inversely related to the amount of formazan and the tested materials showed increasing inhibition of the reduction of NBT as their concentration raised (Figure S5). The IC_{50} values (amount of catalyst required for 50% inhibition of NBT reduction) were determined graphically from the plots of % inhibition *vs* catalyst concentration, and used to calculate the McCord−Fridovich catalytic constants for $O_2^{\bullet-}$ scavenging (k_{McF}) according to $k_{McF} = k_{NBT}$ [NBT] / IC_{50} [39]. These k_{McF} values are independent of the detector concentration and suitable to compare with reported values for other catalysts.

IC_{50} and k_{McF} values for immobilized and host-free complexes are listed in entries 1-6 of Table 2. As can be observed, insertion of dinuclear complexes **1** and **2** via electrostatic forces onto the rigid support supplies better performing immobilized SOD mimics than **3**@MCM-41, a dinuclear complex with a different copper first-shell environment and ligand constraint. Complexes **1** and **2** with the two metal ions bound through the imidazolate bridge, reproduce the structural motif of the active site in the native enzyme. Therefore, the presence of the imidazolate bridge renders a more efficient $O_2^{\bullet-}$ dismutation. In the mechanism proposed for the CuZn-SOD enzyme, one $O_2^{\bullet-}$ anion reduces the Cu(II) center to yield O_2 and Cu(I), and then Cu(I) reacts with a second $O_2^{\bullet-}$ anion to form H_2O_2 and restore the oxidized form of the enzyme [1], as shown in eqs. (2) and (3). Upon reduction of Cu(II) to Cu(I), the imidazolate protonates and dissociates from copper but remains bound to the Zn(II) ion, with the protein framework keeping the Cu(I) and HImZn(II) moieties close to each other. During the reduction of superoxide, ImH^+ acts as a proton source to form H_2O_2.

$$[N_3Zn\text{-}Im\text{-}Cu(II)N_3] + H^+ + O_2^{\bullet-} \rightarrow [N_3Zn\text{-}ImH + Cu(I)N_3] + O_2 \quad (2)$$

$$[N_3Zn\text{-}ImH + Cu(I)N_3] + H^+ + O_2^{\bullet-} \rightarrow [N_3Zn\text{-}Im\text{-}Cu(II)N_3] + H_2O_2 \quad (3)$$

In the hybrid materials, the nanochannels of the mesoporous silica can be envisioned to mimic the protein backbone keeping the Cu active site and HImZn group in close proximity to undergo the reversible transformation between imidazolate-bridged and

nonbridged states, thus facilitating proton transfer from imidazole to $O_2^{\bullet-}$ in the reductive half-reaction. This can account for the significantly higher SOD activity exhibited by **1**@MCM-41 and **2**@MCM-41 compared to the free complexes. An analogue effect was observed for **2-dil**@MCM-41, which showed the same k_{McF} as **2**@MCM-41. In solution, the dienZn(or Cu)ImH^{2+} fragment moves away from the catalytic copper site and proton transfer from imidazole to the $O_2^{\bullet-}$ bound to Cu(I) is much less efficient than inside the pore. By contrast to imidazolate-bridged dinuclear complexes, confinement of **3** in the silica channels has a negative effect on its SOD activity (already poor for the free complex), probably because the pore straitens even more the inherent low flexibility of the N_2O_2-ligand to accommodate Cu(I) [23].

Table 2 shows the SOD activities reported for complexes **1**-**3** encapsulated in mesoporous SBA-15 silica [22] (Entries 7-9). The pore size of this SBA-15 silica is 8.6 nm, larger than the pore diameter of the mesoporous MCM-41 silica employed in the present work. As can be seen, confinement of the imidazolate-bridged complexes in both silicas enhances SOD activity, but MCM-41 with the smaller pore size improves the SOD activity of these compounds more than the host with the larger pore diameter, probably because of the close-fitting of the complexes into the nanochannels that favors the Cu active site and HImZn group stay in closer proximity for proton transfer.

Enhanced SOD activity upon encapsulation had also been observed for [(bipyridinyl)$_2$Cu-μ-pbi-Zn(pbi)](ClO$_4$)$_2$ (**4**, pbi = 2-(2-pyridyl)-benzimidazole) inserted in a dye-functionalized mesoporous silica with 2.5 nm pore size [40], and [(dien)Cu(μ-Im)Zn(tren)]$^{3+}$ [41] (**5** = tren = tris(2-aminoethyl)amine) immobilized in silica gel [21] or Al-MCM-41-N$^+$ [19], a mesoporous aluminosilicate with positively charged surface and 2.5 nm pore diameter (Table 2, entries 10-14). In all the hybrid materials listed in Table 2, the Cu(II) center is less distorted (*f*-factor from 115 to 135) than the local environment of the native enzyme (*f*-factor = 160) and this could account for their relative SOD activities compared to the enzyme (Table 2, entry 15).

Table 2. SOD activity of free and immobilized complexes

Entry	Catalyst	IC_{50} [μM]	k_{McF} [M^{-1} s^{-1}]	Ref.
1	**1**@MCM-41	0.044	62.1×10^6	This work
2	**2**@MCM-41	0.053	51.5×10^6	This work
3	**3**@MCM-41	4.61	0.59×10^6	This work
4	**1**	0.423	6.46×10^6	[23]
5	**2**	0.35	7.80×10^6	[23]
6	**3**	3.2	0.85×10^6	[23]
7	**1**@SBA-15		25.1×10^6	[22]
8	**2**@SBA-15		23.5×10^6	[22]
9	**3**@SBA-15		0.456×10^6	[22]
10	**4**		6.69×10^6 [a]	[40]
11	**4**@MSN-FITC		65.3×10^6 [a]	[40]
12	**5**		4.30×10^6 [a]	[41]
13	**5**@silica gel		49.5×10^6 [a]	[21]
14	**5**@Al-MCM-41-N^+		156×10^6	[19]
15	CuZn-SOD (native)		1800×10^6	[42]

[a]Calculated from reported data using k_{NBT} (pH = 7.8) = 5.94 x 10^4 M^{-1} s^{-1} [39]. **4** = $[(bipyridinyl)_2Cu\text{-}\mu\text{-}pbi\text{-}Zn(pbi)](ClO_4)_2$, pbi = 2-(2-pyridyl)-benzimidazole. FITC = fluorescein isothiocyanate, MSN = mesoporous silica nanoparticles. **5** = [(dien)Cu(μ-Im)Zn(tren)]$^{3+}$, tren = tris(2-aminoethyl)amine.

4. CONCLUSIONS

Encapsulation of the diphenoxo-bridged CuZn complex **3** in silica with small pore size is ineffective for $O_2^{\bullet-}$ dismutation. This complex can be inserted inside the pores of MCM-41 silica successfully but shows SOD activity significantly lower than the host-free

complex, probably because the silica channels restraint the stereochemical rearrangement of the rigid doubly-bridged dinuclear complex to meet a trigonal planar co-ordination around the Cu(I) center. In contrast, insertion of the imidazolate-bridged CuZn or Cu_2 complexes by ion exchange onto mesoporous MCM-41 silica affords durable and recoverable supported catalysts with better SOD activity than the free complexes. This higher efficiency can be attributed to the mesoporous matrix that mimics the protein framework not only to isolate the catalyst and protect it from the external medium, but mainly to avoid the copper redox center and imidazole moieties shift away. The last effect is enhanced by mesoporous MCM-41 silica with small pore size which is best suited to keep the two catalyst' fragments close to each other during catalysis. Since the geometrical environment of the Cu(II) center remains practically unaffected after insertion into the MCM-41 silica matrix (similar *f*-factor), the SOD activity improvement of imidazolate-bridged **1** and **2** upon encapsulation should be mostly due to the confinement in the small pores.

Acknowledgments

This work was supported by the National University of Rosario (PI BIO553) and the Consejo Nacional de Investigaciones Científicas y Técnicas (CONICET, PIP 0337), the Centre National de la Recherche Scientifique (CNRS, PICS 07121), and the Agency for Science, Technology and Innovation of Santa Fe (ASACTeI, IO 2010-164-16). We acknowledge ESRF for provision of synchrotron radiation on the FAME beamline (Proposal 30-02-1078 and 30-02-1126), the FAME team and Dr. Laurent Sabater for his participation in data recording.

Apendix A- Supplementary data

Supplementary data associated with this article can be found, in the online version, at http://dx.doi.org/10.1016/j.jinorgbio.xxxx.

REFERENCES

[1] I. A. Abreu, D. E. Cabelli, Biochim. Biophys. Acta 1804 (2010) 263–274.

[2] M. Hayyan, M. A. Hashim, I. M. AlNashef, Chem. Rev. 116 (2016) 3029−3085.

[3] C. Cheignon, M. Tomas, D. Bonnefont-Rousselot, P. Faller, C. Hureau, F. Collin, Redox Biology 14 (2018) 450-464.

[4] S. G. Rhee, T.-S. Chang, W. Jeong, D. Kang, Mol. Cells 29 (2010) 539–549.

[5] Y. Sheng, I. A. Abreu, D. E. Cabelli, M. J. Maroney, A.-F. Miller, M. Teixeira, J. S. Valentine, Chem. Rev. 114 (2014) 3854–3918.

[6] D. Salvemini, C. Muscoli, D.P. Riley, S. Cuzzocrea, Pulm. Pharmacol. Ther. 15 (2002) 439–447.

[7] D. P. Riley, Chem. Rev. 99 (1999) 2573–2588.

[8] C. Policar, in: J. S. Reboucas, I. Batinic-Haberle, I. Spasojevic, D. S. Warner, D. St., Clair (Eds.), Redox Active Therapeutics, Springer, Berlin, 2016, pp. 125– 164.

[9] S. Signorella, C. Palopoli, G. Ledesma, Coord. Chem. Rev. 365 (2018) 75–102.

[10] I. I. Slowing, J. L. Vivero-Escoto, B. G. Trewyn, V. S. Y. Lin, J. Mater. Chem. 20 (2010) 7924-7937.

[11] L. Du, J. Li, C. Chen, Y. Liu, Free Radical Res. 48 (2014) 1061-1069.

[12] F. P. Chang, Y. P. Chen, C. Y. Mou, Small 10 (2014) 4785-4795.

[13] R. Diab, N. Canilho, I. A. Pavel, F. B. Haffner, M. Girardon, A. Pasc, Adv. Colloid Interface Sci. 249 (2017) 346-362.

[14] G. Martínez-Edo, A. Balmori, I. Pontón, A. Martí del Rio, D. Sánchez-García, Catalysts 8 (2018) 617.

[15] N. Zhao, L. Yan, X. Zhao, X. Chen, A. Li, D. Zheng, X. Zhou, X. Dai, F.-J. Xu, Chem. Rev. 119 (2019) 1666-1762.

[16] A. Heuer-Jungemann, N. Feliu, I. Bakaimi, M. Hamaly, A. Alkilany, I. Chakraborty, A. Masood, Ma. F. Casula, A. Kostopoulou, E. Oh, K. Susumu, M. H. Stewart, I. L. Medintz, E. Stratakis, W. J. Parak, A. G. Kanaras, Chem. Rev. 119 (2019) 4819−4880.

[17] B. Albela, L. Bonneviot, New J. Chem. (2016) 4115-4131.

[18] C.-H. Lee, S.-T. Wong, T.-S. Lin, C.-Y. Mou, J. Phys. Chem. B 109 (2005) 775-784.

[19] Y.-C. Fang, H.-C. Lin, I-J. Hsu, T.-S. Lin, C.-Y. Mou, J. Phys. Chem. C 115 (2011) 20639–20652.

[20] I. Szilágyi, I. Labádi, K. Hernadi, T. Kiss, I. Pálinkó Stud. Surf. Sci. Catal. 158 (2005) 1011-1018.

[21] I. Szilágyi, I. Labádi, K. Hernadi, I. Pálinkó, I. Fekete, L. Korecz, A. Rockenbauer, T. Kiss, New J. Chem. 29 (2005) 740-745.

[22] M. Patriarca, V. Daier, G. Camí, N. Pellegri, E. Rivière, C. Hureau, S. Signorella, Micropor. Mesopor. Mat. 279 (2019) 133-141.

[23] V. A. Daier, E. Rivière, S. Mallet-Ladeira, D. Moreno, C. Hureau, S. R. Signorella, J. Inorg. Biochem. 163 (2016) 162-175.

[24] K. Suzuki, K. Ikari, H. Imai, J. Am. Chem. Soc. 126 (2004) 462-463.

[25] K. Ikari, K. Suzuki, H. Imai, Langmuir 22 (2006) 802-806.

[26] O. Proux, X. Biquard, E. Lahera, J. J. Menthonnex, A. Prat, O. Ulrich, Y. Soldo, P. Trévisson, G. Kapoujvan, G. Perroux, P. Taunier, D. Grand, P. Jeantet, M. Deleglise, J.-P. Roux, J.-L. Hazemann, Phys. Scr. 115 (2005) 970–973.

[27] C. Beauchamps, I. Fridovich, Anal. Biochem. 44 (1971) 276–287.

[28] V. Daier, D. Moreno, C. Duhayon, J.-P. Tuchagues, S. Signorella, Eur. J. Inorg. Chem. (2010) 965–974.

[29] P.J. Branton, P.G. Hall and K.S.W. Sing, J. Chem. Soc., Chem. Commun. (1993) 1257-1258.

[30] Sing K. S. W. Adv Colloid Interface Sci. 76-77 (1998) 3-11.

[31] R. N. Patel, N. Singh, K. K. Shukla, U. K. Chauhan, CCDC 203653: Experimental Crystal Structure Determination, 2005.

[32] L. S. Kau, D. J. Spira-Solomon, J. E. Penner-Hahn, K. O. Hodgson, E. I. Solomon, J. Am. Chem. Soc. 109 (1987) 6433–6442.

[33] S. Della Longa, I. Ascone, A. Bianconi, A. Bonfigli, A. Congiu Castellano, A. Zarivi, M. miranda, J. Biol. Chem. 271 (1996) 21025-21030.

[34] E. Borghi, P. I. Solari, M. Beltramini, L. Bubacco, P. Di Muro, B. Salvato, Biophys J. 82 (2002) 3254-3298.

[35] L. Giachini, G. Veronesi, F. Francia, G. Venturolid, F. Boscherinib, J. Synchrotron Radiat. 17 (2010) 41– 52.

[36] J. Osán, F. Meirer, V. Groma, S. Török, D. Ingerle, C. Streli, G. Pepponi, Spectrochim. Acta Part B 65 (2010) 1008-1013.

[37] C. G. Palivan, V. Balasubramanian, B. A. Goodman, Eur. J. Inorg. Chem. (2009) 4634–4639.

[38] J. Shearer, L.M. Long, Inorg. Chem. 45 (2006) 2358–2360.

[39] Z. R. Liao, X. F. Zheng, B. S. Luo, L. R. Shen, D. F. Li, H. L. Liu, W. Zhao, Polyhedron 20 (2001) 2813–2821.

[40] Y.-C. Fang, Y.-P. Chen, .C.-T. Chen, T.-S. Lin, C.-Y. Mou, J. Mater. Chem. B 1 (2013) 6042-6052.

[41] I. Szilágyi, I. Labádi, K. Hernadi, I. Pálinkó, N. V. Nagy, L. Korecz, A. Rockenbauer, Z. Kele, T. Kiss, J. Inorg. Biochem. 99 (2005) 1619–1629.

[42] G. Rotilio, R. C. Bray, E. M. Fielden, Biochim. Biophys. Acta 268 (1972) 605-609.